tvst

Article

Noninvasive and Noncontact Sequential Imaging of the Iridocorneal Angle and the Cornea of the Eye

Xun Jie Jeesmond Hong[1], C. S. Suchand Sandeep[1,2], V. K. Shinoj[1,#], Tin Aung[3,4], Veluchamy Amutha Barathi[3,4,5], Mani Baskaran[3,5], and Vadakke Matham Murukeshan[1]

[1] Centre for Optical and Laser Engineering, School of Mechanical and Aerospace Engineering, Nanyang Technological University, Singapore
[2] Singapore Centre for 3D Printing, School of Mechanical and Aerospace Engineering, Nanyang Technological University, Singapore
[3] Singapore Eye Research Institute (SERI) & Singapore National Eye Center (SNEC), Singapore
[4] Department of Ophthalmology, Yong Loo Lin School of Medicine, National University of Singapore, Singapore
[5] The Ophthalmology & Visual Sciences Academic Clinical Program, Duke-NUS Medical School, Singapore
[#] Currently with Union Christian College, Department of Physics, Kerala, India

Correspondence: Mani Baskaran, Singapore Eye Research Institute (SERI), The Academia, 20 College Road, Discovery Tower Level 6, 169856 - Singapore. . e-mail: baskaran.mani@seri.com.sg
Vadakke Matham Murukeshan, School of Mechanical and Aerospace Engineering, 50 Nanyang Avenue, Nanyang Technological University, 639798 - Singapore. e-mail: mmurukeshan@ntu.edu.sg

Received: September 9, 2019
Accepted: December 22, 2019
Published: April 9, 2020

Keywords: aqueous outflow system; iridocorneal angle; trabecular meshwork; high-resolution imaging; Bessel beam; light sheet fluorescence microscopy; cornea; ocular imaging; glaucoma

Citation: Hong XJJ, Suchand Sandeep CS, Shinoj VK, Aung T, Barathi VA, Baskaran M, Murukeshan VM. Noninvasive and noncontact sequential imaging of the iridocorneal angle and the cornea of the eye. Trans Vis Sci Tech. 2020;9(5):1, https://doi.org/10.1167/tvst.9.5.1

Purpose: High-resolution imaging of the critical anatomic structures of the eye, especially of the anterior chamber, in vivo, remains a challenge, even with currently available state-of-the-art medical imaging techniques. This study aims for the noninvasive and noncontact sequential imaging of the iridocorneal angle, especially the trabecular meshwork (TM) and the cornea of the eye in high-resolution using a newly developed imaging platform.

Methods: Bessel beam scanned light sheet fluorescence microscopy is used to attain high-resolution images of the TM. The ability of the Bessel beam to self-reconstruct around obstacles increases the image contrast at the TM region inside eye by reducing scattering and shadow artifacts. With minimal modifications, the excitation arm of the developed imaging system is adapted for noncontact, high-resolution corneal imaging.

Results: High-resolution images of the TM structures and cellular-level corneal structures are obtained in ex vivo porcine eyes, and subsequently in New Zealand white rabbit, in vivo. The spatial resolution of the developed system is 2.19 µm and has a noncontact working distance of 20 mm.

Conclusions: A high-resolution imaging platform for noncontact sequential imaging of the TM and the cornea of the eye is developed. This imaging system is expected to be of potential interest in the evaluation and diagnosis of glaucoma and corneal diseases.

Translational Relevance: The developed prototype offers the plausibility of in vivo, noncontact, and high-resolution imaging of the iridocorneal angle and cornea of the eye that will aid clinicians in diagnosing open-angle glaucoma and corneal diseases better.

Introduction

For the early and accurate detection of glaucoma and corneal diseases, high-resolution imaging modalities are essential. Diagnostic medical instrumentations based on optical methodologies allow high-resolution imaging and ultrasensitive detection. These photographic and optical tomographic imaging modalities have significant contributions to the diagnosis, prognosis, and management of glaucoma and corneal diseases. Nonetheless, they all have both benefits and drawbacks in acquiring repeatable and reliable measurements. In this context, this article reports a potential noninvasive, noncontact method and apparatus for the sequential imaging of the cornea and iridocorneal angle (ICA), which can complement existing imaging modalities with high-resolution images.

Abnormalities in the aqueous outflow system (AOS) of the eye can result in an elevated intraocular pressure, which can subsequently cause glaucoma, a disease resulting from damage to optic nerve that may lead to permanent loss of vision.[1] Glaucoma is also known as the "silent thief of sight" because the initial vision loss is mainly peripheral and not readily noticeable. Treatment for glaucoma includes pharmacologic therapy, laser-based therapy, and surgery. However, being a chronic condition, glaucoma requires continuous review even after the intraocular pressure is well-regulated. The aim of the treatment is to preserve the remaining vision, because damage from glaucoma to the optic nerve cannot be reversed.

The imaging of anatomic structures in the anterior chamber of the eye, in vivo, is a challenge, even with today's state-of-the-art medical technology.[2] A vital part of the AOS in the eye is the ICA, which comprises the trabecular meshwork (TM) and the Schlemm's canal. Clinicians primarily rely on individualized approaches for the assessment of the ICA as there is no universal and foolproof concept or methodology available for imaging the ICA. For example, anterior segment optical coherence tomography (AS-OCT)[3,4] is a method used by clinicians to detect eyes with narrow angles. AS-OCT helpful in obtaining quantitative information about the angle width and can be used to observe pathologic changes overtime. Although AS-OCT can image different structures of the anterior segment and can be used to quantify the TM region, it is unable to image the individual TM structures.[5–7] Even studies dedicated to TM imaging using polarization-sensitive OCT were not able to resolve the individual TM structures.[6] Another method used for the angle imaging is ultrasound biomicroscopy (UBM),[8] which is also able to image structures posterior to the iris. This method is also not capable of imaging the individual TM structures owing to lack of resolution. Researchers are working on new devices and instrumentation for imaging the AOS.[9] Such imaging modalities must have adequate spatial resolution (approximately 1–5 μm) and contrast to resolve the TM structures, to be of greater diagnostics value toward the understanding of the disease state, and evaluation of treatments that decrease intraocular pressure.

Corneal diseases are another leading cause of blindness, together with glaucoma and cataract.[10,11] They include a wide range of inflammatory and infectious diseases that can cause corneal scarring and eventually lead to loss of vision. Corneal inflammation can occur from many factors, such as ocular trauma, ocular surface diseases, corneal sutures, previous ocular surgery, eyelid malalignment, and even from diseases unrelated to the eye, such as diabetes. The success rate of surgical intervention of corneal blindness is good, but can be affected by postoperative complications and graft rejection. For corneal inspection, the most advanced imaging system that provides cellular level resolution is the in vivo laser scanning confocal microscopy (LSCM).[12] LSCM can image most of the corneal structures in vivo and helps clinicians to evaluate the disease state and treatment response without any physical sectioning. However, most of the LSCM instruments available for ocular imaging are contact based and hence there is a risk of corneal injury and applanation of the cornea that introduce artifacts in the images. UBM is another commonly used tool used for corneal pachymetry. UBM can image the anterior segment of the eye even in the presence of scarred and edematous corneal tissues. However, being a contact technique, UBM is also is impractical in many clinical situations such as in the case of eyes with ocular injuries and postoperative eyes. It may also cause distortion to the eye anatomy due to the supine positioning of the patient during image acquisition.[13] Both UBM and LSCM require experienced and skilled operators for obtaining high-quality images and to minimize the risk of corneal infections or abrasions. Emerging technology based on multiphoton microscopy[14] is promising, offering a greater depth of penetration and lower photo toxicity compared to conventional confocal system. Recently a safe in vivo technique using two-photon microscopy has been reported for the noninvasive imaging of the eye.[15] Nonetheless, there remains an extensive amount of translational and clinical investigation necessary before its integration into clinical ophthalmology. AS-OCT is the gold standard in measuring the anterior segment of the eye.[16] AS-OCT is a well-established technique, but routinely only measures cross-sectional data. The en face images need to be reconstructed

Table 1. Process for *Need Statement* Conceptualization Addressing Glaucoma

Clinical observation	Imaging the critical anatomic structures of the eye, especially of the anterior chamber, in vivo, remains a challenge, even with currently available state-of-the-art medical imaging techniques. The lack of visualization tools for characteristic anatomic structures such as the Schlemm's canal, the TM, and scleral spur, severely restrict clinicians and vision researchers, in obtaining objective information that can help in the detection and evaluation of primary open angle and angle closure glaucoma.
Problem identification	Clinicians rely on individual approaches for ICA assessment, as there is no universal, foolproof methodology for imaging the ICA. These approaches usually result in higher financial burden on the patients.
Need Statement conceptualization	There is a need for high-resolution (approximately 1 – 5 μm) imaging method that is capable of resolving the TM structures, to be of greater diagnostics value toward the understanding of the disease state, and subsequent treatments that decrease intraocular pressure.

Table 2. Process for *Need Statement* Conceptualization Addressing Corneal Diseases

Clinical observation	Currently available commercial ophthalmology instruments for corneal imaging are associated with limitations such as the dependence on coupling medium, insufficient resolutions, long image acquisition times, the need for trained and experienced operators, risk of epithelial injuries, and thus lack of information for detection and evaluation of corneal diseases.
Problem identification	Multiple diagnostic instruments might be necessary with the currently available imaging modalities to image the entire cornea with required resolution. Multiple test procedures result in higher stress and higher financial burden on patients.
Need Statement conceptualization	There is a need for high-resolution imaging methods that are simple, noncontact, and has excellent safety profile for a clinician and patient friendly investigation.

from the cross-sectional images, which is often difficult. There have been exciting advances in en face OCT technology in research that have achieved high-quality, noncontact, cellular-level images of the corneal structures.[17–19] However, commercially available OCT ocular imaging systems lack the cellular resolution en face imaging capabilities. Undoubtedly, there is a need for high-resolution imaging methods that are simple, noncontact, and have an excellent safety profile.

In the context of innovating medical technologies,[20,21] several different gaps can exist in the diagnostics landscape, with each leading to different opportunities. This article focuses on identifying the white space gap, and then conceptualizing ways to align an unrelated technology with the *Need Statement*. Tables 1 and 2 summarize the clinical observations, problem identification, and the *Need Statement* conceptualization for glaucoma and corneal disease, respectively.

This work aims to explore the advantage of Bessel beam[22,23] to form extended range high-resolution images, unattainable by conventional Gaussian beam illumination. Additionally, the ability of the Bessel beam to self-reconstruct around obstacles is expected to increase the image contrast at the TM region inside eye by reducing scattering and shadow artifacts.[24] This research also looked into a corneal high-resolution imaging configuration that provides diagnostic information for corneal related diseases. With minor modifications, the excitation arm of the proposed ICA imaging system can be adapted for high-resolution corneal imaging. Although we have reported the Bessel beam light sheet fluorescence microscopy (LSFM)–based ICA imaging system and Gaussian beam based corneal imaging system in the past,[25,26] a method to integrate these two techniques to a single system that can be used for both corneal imaging and ICA imaging is reported in this work. Further the in vivo and ex

vivo imaging capabilities of this system are also demonstrated as proof of concept. The in vivo imaging of TM using this technique is being reported for the first time. This optical configuration is expected to be useful among researchers and clinicians for the evaluation and diagnosis of corneal diseases and glaucoma.

Methods

Materials

Analytical-grade reagents were used for the preparation of porcine eye samples. Sodium hydroxide pellets were obtained from Merck (Kenilworth, NJ) and fluorescein powder was obtained from Fluka Analytical/Sigma-Aldrich (St Louis, MO). Millipore (Burlington, MA) water (resistivity 18.2 MΩ cm, from the Milli-Q Synthesis A10) was used for making the solutions. For the animal models, medical grade fluorescein eye drops (Minims Fluorescein Sodium 2%; Bausch & Lomb, Kingston upon Thames, UK) were applied.

Preparation of Porcine Eye Samples

The porcine eye samples were procured from a local abattoir from 15 randomly selected pigs (*Sus scrofa domestica*) and were used within 2 hours after extraction. A custom designed eye holder mounted on an X–Y translation stage was used for holding the samples during the measurements.

Preparation of Fluorescein Dye

Because the fluorescein powder is insoluble in water, 0.02 g fluorescein was dissolved in 10 mL of 1 M sodium hydroxide to prepare the 0.2 % w/v of fluorescein sodium solution. To prevent photobleaching, this dye solution was stored in the dark. The anterior chambers of the porcine eye samples were injected with the fluorescein dye using a 29-gauge needle syringe.

Preparation of New Zealand White (NZW) Rabbit

One randomly selected eye of the NZW rabbit was applied with medical grade 2% fluorescein sodium eye drops solution 4 hours before the start of the experiment. Three doses of fluorescein sodium eye drops were applied, at an interval of 5 minutes. The excess dye was washed off with saline solution. The NZW rabbit was anesthetized intramuscularly with a combination of ketamine hydrochloride (50 mg/kg) and xylazine (10 mg/kg). The rabbit's eyelids were manipulated using suitable eyelid retractors.

All in vivo imaging measurements were conducted at the Singapore Eye Research Institute (SERI), SingHealth Experimental Medicine Centre. All the experiments were approved by the Institutional Animal Care and Use Committee (IACUC, approval number: 2014/SHS/928). All animal research was conducted in compliance with the ARVO Statement for the Use of Animals in Ophthalmic and Vision Research.

Fluorotron Master (Ocumetrics, Mountain View, CA) was used to measure the fluorescein level within the rabbit's eye. This instrument can construct fluorescein concentration profiles from the cornea to the retina, by sequentially focusing on spatially distinct sites along the ocular axis.[27] The data were processed and displayed graphically (Fig. 1).

Experimental Setup for the Sequential Imaging of the ICA Region and Cornea

For the interrogation of the ICA region, a 488 nm diode laser (LuxX 488, Omicron, Berlin, Germany) was used as the excitation source and the fluorescence signal emitted from the TM network was detected by a scientific complimentary metal-oxide semiconductor detector (Andor Neo 5.5, Andor Technology; Belfast, UK). The output from the fiber coupled excitation laser was collimated using a preassembled fiber collimator (F810FC-543; Thorlabs Inc., Newton, NJ) and was made incident onto a planoconvex axicon lens (176° apex angle; Altechna Co. Ltd., Vilnius, Lithuania). The ring phase of the generated Bessel beam was then collimated and directed to a Galvano scanner (Cambridge Technology Inc., Bedford, MA) and relayed to a 20× objective lens (numerical aperture [NA] = 0.42, infinity-corrected, 20 mm working distance; Mitutoyo corp., Kanagawa, Japan) using a visible scan lens (CLS-SL, 54 mm working distance, f = 70 mm; Thorlabs Inc.), and a tube lens (ITL200, infinity corrected, 148 mm working distance, f = 200 mm; Thorlabs Inc.) combination. Another infinity-corrected objective and tube lens configuration was used to collect the fluorescence emitted from the TM to the highly sensitive scientific complementary metal-oxide semiconductor camera. The imaging arm was placed orthogonal to the illumination axis. The 488 nm notch filter (center wavelength = 488 nm, full width at half maximum 15 nm) was placed within the infinity space in the detection axis to attenuate the 488 nm excitation wavelength, while transmitting the 520 nm emission wavelength of fluorescein sodium. A variable neutral density filter was

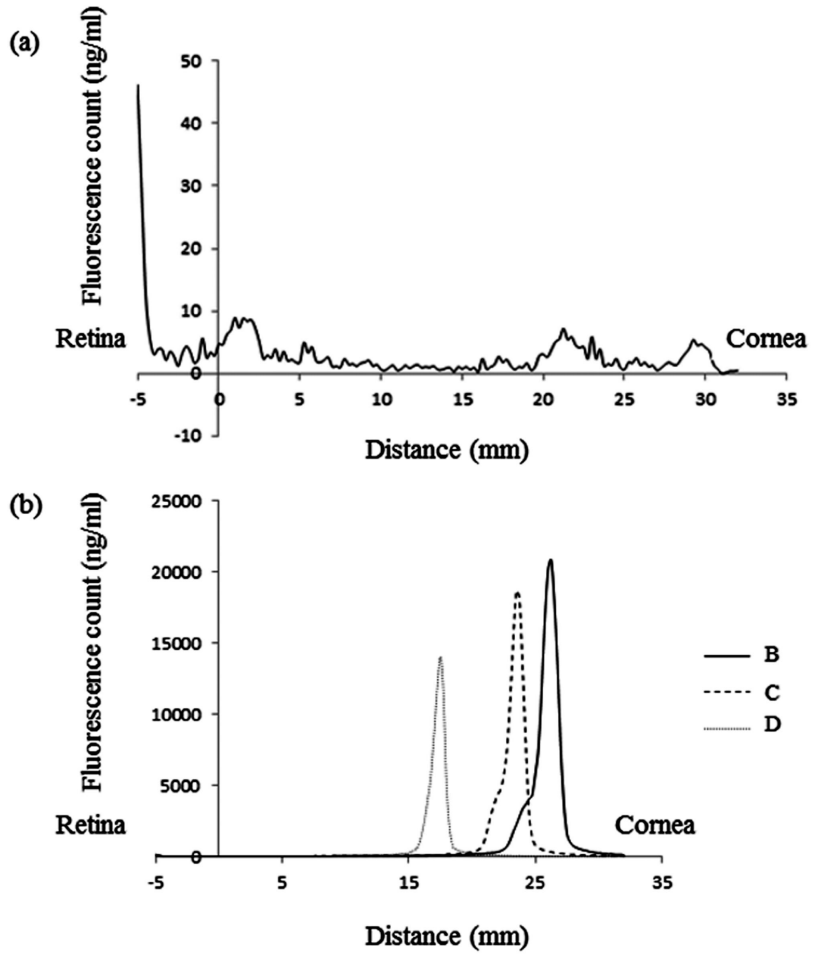

Figure 1. Fluorotron Master data showing (a) background level of fluorescence count in an untreated eye of the NZW rabbit, and (b) fluorescence count in the same eye after fluorescein is applied. The three different plots in (b) represent three independent scans targeted at different depths of the eye.

used to control the light intensity falling on the camera and a USB digital microscope (Dino-Lite Pro, Taipei, Taiwan) was installed to assess and document the alignment of the laser beam. Figure 2 shows a schematic of the experimental setup. A photograph of the prototype can be found in Supplementary Figure S1.

Imaging Method for ICA Region

Generating the Bessel beam using an axicon lens is more efficient in comparison with other conventional methods.[28] Additionally, photobleaching and photodamage can be minimized in this case because higher illumination efficiency equates to lower exposure time. There is also potential for super resolution imaging, as the radius of the central spot of the Bessel beam ($|J_0|^2$) is approximately 38% smaller than the first dark ring of the Airy pattern for an infinitely small annular width.[29] The formation of a Bessel beam using an axicon and subsequent propagation through a 4f system is illustrated in Figure 3.

The depth of focus, Z_D, of the Bessel beam in this scheme can be controlled by a variable aperture placed before the axicon surface, and is given by the following equation[28]:

$$Z_D = \frac{R_{ill}}{(n-1)_\gamma} \tag{1}$$

where R_{ill} is the radius of the incident beam, and n and γ are the refractive index and the cone angle of the axicon, respectively. From this equation, it can be seen that Z_D and R_{ill} are directly proportional. Careful selection of the aperture size to control Z_D, to ensure that only the region of interest is precisely illuminated, is necessary to keep the side lobe excitation tails around the central core to minimum. By scanning the vertical mirror of the Galvano scanner, a virtual Bessel light sheet can be achieved. Because there is no beam-shaping aperture in the generation of the

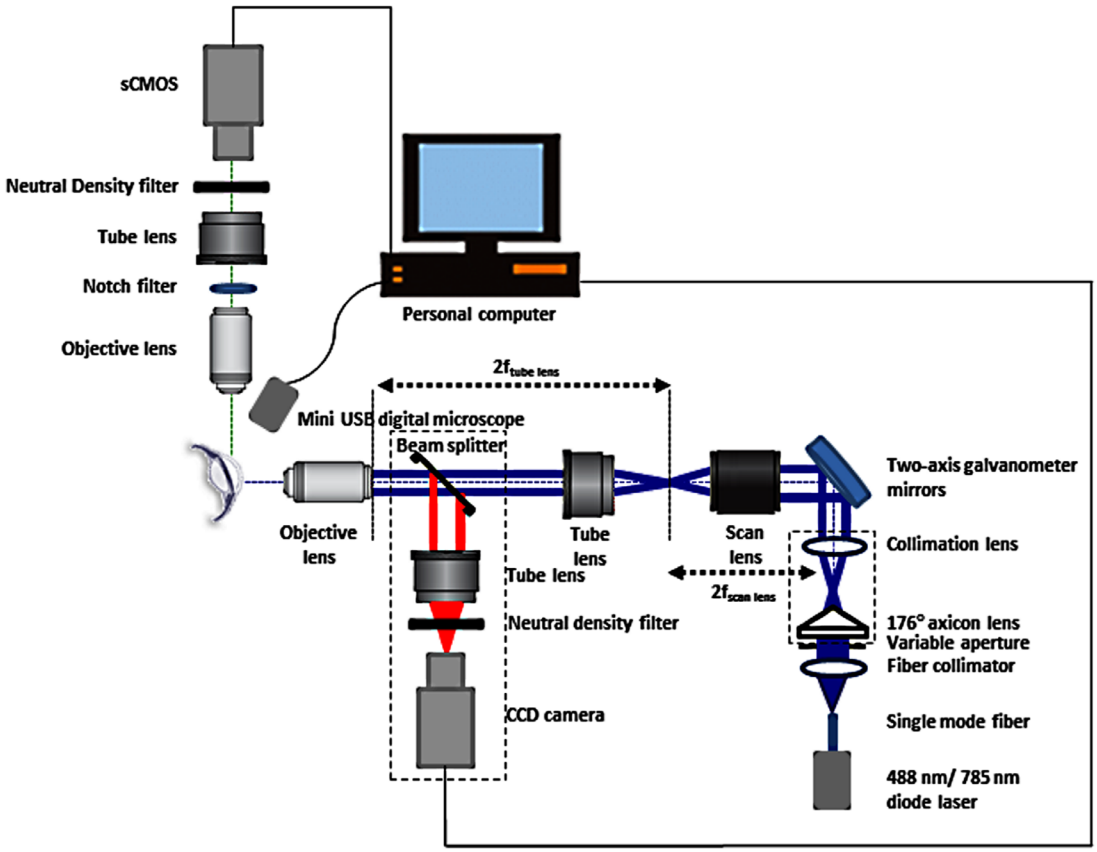

Figure 2. The combined experimental setup for the sequential imaging of the ICA region and the cornea. For corneal imaging a diode laser of 785 nm wavelength was used, and the axicon and collimation lens were removed. CCD, charge coupled device; sCMOS, scientific complementary metal-oxide semiconductor.

light sheet, optical aberrations associated with beam-shaping apertures need not be considered.[30] The intrinsic self-reconstructing capability of the Bessel beam enhances the imaging contrast deep inside the highly light-scattering structures of the ICA. The scanning scheme helps to decrease photobleaching and the acquisition time and lowers the patient's discomfort. Furthermore, the noncontact nature of the proposed system, owing to the use of long working distance objectives, gives it an added advantage over the traditional contact based ICA imaging techniques such as gonioscopy.

The position of the illumination light sheet should be aligned to be within the depth of field of the imaging objective (Fig. 4). This positioning ensures that the light is concentrated only at the region of interest, resulting in an efficient illumination. Additionally, this positioning improves the image sharpness and reduces background noise.[26] The proposed LSFM scheme has an intrinsic optical sectioning capability, because no fluorescence is generated beyond the illumination plane, minimizing the out-of-focus background.

The use of infinity optics in the proposed system helps in maintaining the parfocality of the system and also ensures that no spherical aberrations or change in working distance are introduced by optical components placed in the infinity space. Since the notch filter is placed into a parallel flux of light waves, both the location and focal point of the image remain unchanged, and the 20× magnification is maintained throughout the compound lens system in the detection arm.

Imaging Method for Cornea

A diode laser of 785 nm wavelength (LBX-785, Oxxius, Lannion, France) was used for corneal imaging and the fiber collimator F810FC-543, was replaced by F810FC-780. Because these preconfigured fiber collimators are designed for a specific wavelength, it becomes necessary to change the collimator to match the excitation light source for optimal performance. The axicon and collimation lens were removed in the corneal imaging scheme. In contrast with the

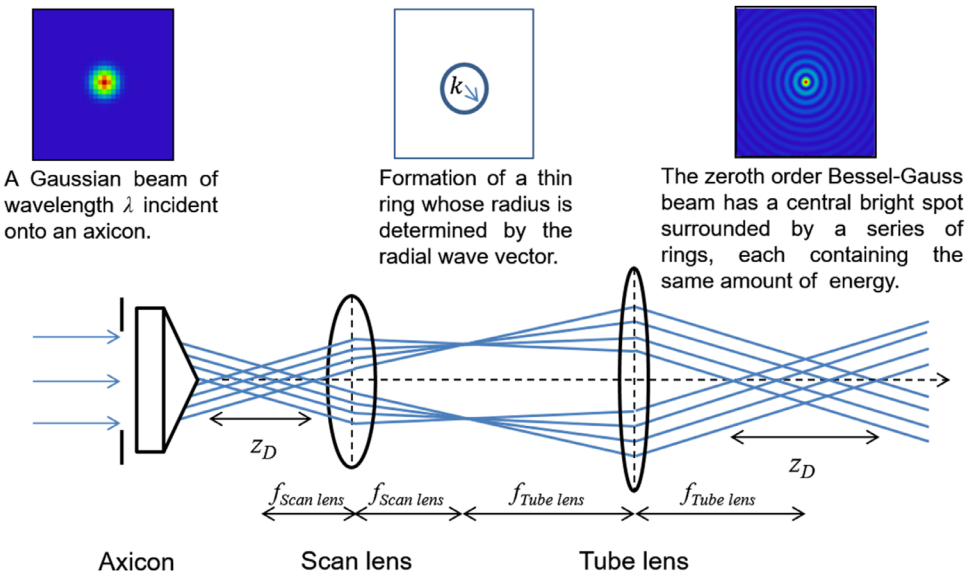

Figure 3. Illustration of a Bessel beam formation through a series of lens arranged in a 4F configuration. The axicon is illuminated with a Gaussian beam of wavelength λ.

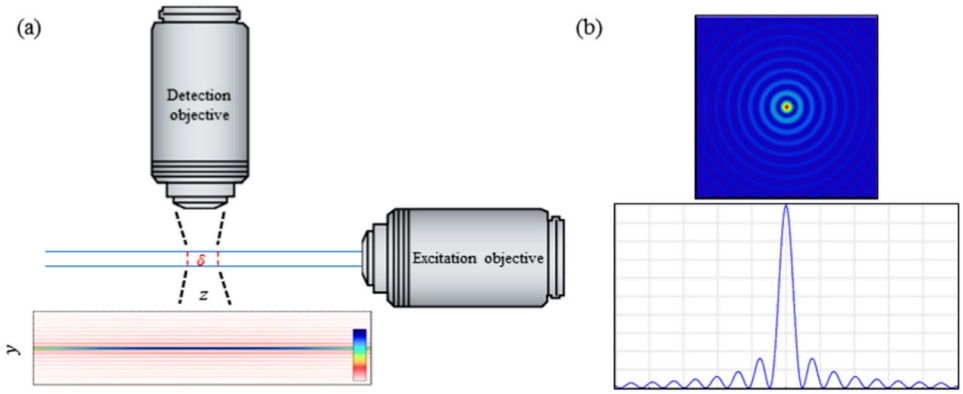

Figure 4. The projection of a Bessel beam into the FOV of the detection objective. The Bessel beam has a longer depth of focus and a central peak that is narrower than the Gaussian beam. (b) The relative intensity (amplitude squared) cross-section of a Bessel beam and its relative radial intensity.

orthogonal excitation configuration in LSFM, the corneal imaging scheme is based on an epi-illumination configuration. In the epi-illumination scheme, the images are collected by the same objective lens that is used for illuminating the sample and then reflected by the pellicle beam splitter in the illumination path. A CMOS camera (PL-B741; PixeLINK, Ottawa, Ontario, Canada) in combination with an infinity-corrected tube lens was used to record the reflected images. To control the intensity of light falling on the CMOS camera, a neutral density filter was used and the images were directly displayed on the computer monitor. The objective lens was moved toward the sample and image capturing was initiated when the first superficial cells of the cornea became visible. The same Dino-Lite USB microscope used for ICA imaging was used to record the alignment of the laser beam.

The objective lens was moved using a translation stage with micrometer precision for depth-sensitive imaging of targeted region. In this way, the images are recorded by gradually moving the focal plane into the corneal stroma and endothelium. Owing to the greater optical path length (OPL) through the cornea as a result of its higher refractive index, the focal plane shift inside cornea will be different from the actual distance moved by the objective lens. If d is the distance moved by the objective and n is the refractive index of the cornea, the OPL inside the cornea can be calculated using the formula, $OPL = nd$. For example, for every 100 µm shift of the objective, the focal plane inside the

cornea will be shifted by a distance of 137.6 µm along the optical axis (n_{cornea} approximately = 1.376). It must be noted that, for large area interrogation, the curvature of the corneal surface and the associated OPL changes also need to be considered.

Results and Discussion

Choice of Animal Models

The ICA anatomy of the various animal models differs extensively with that from the humans. The development of the anatomic structures is ranked phylogenetically from Rodentia (rabbit), Ungulata (pig), to Primata (subhuman primate).[31] Despite the structural differences, all these animal models have a continuous endothelial lining of the aqueous outflow channels, similar to those in human. Based on the similarity in morphology to human eyes, porcine eyes were chosen as the ex vivo animal model in this study. Porcine eyes have been routinely used in vision research for glaucoma[32] and corneal transplant studies.[33] The corneal thickness (twice that of human cornea) and absence of the Bowman's layer are two major differences in the anterior segment of the porcine eye in comparison to a human eye.[34]

The choice of NZW rabbit as an in vivo animal model was based on the fact that it is a natural glaucoma model[35] and owing to the similarity in cornea size with human.[36] It should be noted that the anterior chamber depth and corneal thickness of the NZW rabbits are slightly lower than those of humans. Although the Descemet and Bowman's layers are not well-developed in rabbits, similar endothelium, stroma and epithelium layers were found in rabbit and human corneas.[37]

ICA Imaging

The challenges of three-dimensional (3D) in vivo imaging should be put into consideration when conceptualizing new imaging modalities for the high-resolution imaging of the AOS. These challenges include the ability to image at cellular/subcellular spatial resolution, optical sectioning capability, high imaging speed, and in the case where fluorescence is required, a low level of photobleaching and photodamage. In addition, they should also have safety profile that is similar to the current state-of-the-art medical instruments.

In the LSFM imaging modality, the lateral and axial resolutions are decoupled and are dependent on the NA of the detection objective and the thickness of the light sheet respectively. The effective lateral resolution of the proposed scheme is given by $\lambda_{ex}/(2NA_{det})$, where λ_{ex} is the wavelength of excitation and NA_{det} is the NA of the detection objective. Typically, for obtaining a large field of view (FOV), lenses with low NA are used. However this results in the reduction of lateral resolution. For the proposed experimental scheme, we used a 20×, long working distance objective with a NA of 0.42. The lateral spatial resolution of this system was determined experimentally by imaging a US Air Force bar target (USAF1951 chart). As shown in Figure 5, the proposed configuration can image up to group 7, element 6, corresponding to a lateral resolution of about 2.19 µm.

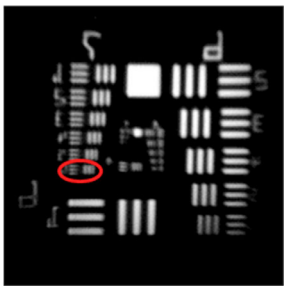

Figure 5. Measurement of lateral resolution using USAF (1951) chart with the 20× objective lens.

Axial resolution measures the smallest distance in the axial direction where two features can be clearly resolved when there is negligible noise, whereas the optical sectioning capability assesses the ability of the imaging system to reject out-of-focus fluorescence signal. These two parameters are related such that an increasing fluorescence signal from poor optical sections results in an axial resolution that is lower than the ideal theoretical value. The axial resolution and optical sectioning capability of the proposed method is defined by the convolution of conventional wide-field detection optical transfer function. The inherent disadvantage of conventional widefield detection methodology is that the detection optical transfer function has a missing cone of axial information, and this results in poor optical sectioning capability and considerable out-of-focus background. In Bessel beam plane illumination, the optical transfer function of the excitation plane (determined by the Bessel beam and the microscope's mode of operation) is able to fill up this missing axial information, hence enhancing the practical limit of the axial resolution and reducing the out-of-focus background. One limiting factor is, however, the deterioration of the illumination quality as a result of the sample-induced aberration or scattering. This limitation undermines the image resolution.

Table 3. Challenges Associated with 3D In Vivo Fluorescence Imaging and the Advantages of the Proposed System

Challenges	Description	Advantages of Proposed System
Cellular/subcellular spatial resolution	Micrometer and submicrometer spatial resolution is required to identify cellular and subcellular ocular imaging in a 3D environment.	Scanned Bessel beam generates much thinner light sheet, resulting in better axial resolution.
Optical sectioning	Excellent optical sectioning allows high signal-to-noise ratio images and at the same time minimizes out-of-focus background on densely labeled or thick samples.	The confined plane of excitation in LSFM will automatically exclude the out-of-focus excitation, providing good optical sectioning capability.
Imaging speed	High imaging speed helps in capturing the cellular/subcellular dynamics.	The simultaneous excitation across the entire illumination plane translates to a high acquisition speed, comparable to conventional wide field imaging.
Photobleaching and photodamage	Photobleaching and photodamage should be as low as possible, so that the samples can be examined over a long period of time, thus revealing the true physiological process in the undisturbed state.	The high imaging speed and scanned light sheet consequently results in lower photobleaching and photodamage.

LSFM, with orthogonal illumination and detection axes, is a potential methodology to bridge the gap between the high penetration, but low-resolution ultrasound imaging and high-resolution but limited penetration of confocal microscopy. LSFM can generate large FOV two-dimensional optical sections with minimal photodamage, because only the plane under observation is selectively illuminated. The minimal exposure time to excitation radiation and the fast image acquisition speed makes LSFM a perfect tool for in vivo ocular imaging. Because the proposed method is noncontact in nature and the eye is positioned upright during the measurements, the eye anatomy is undisturbed, and hence it is possible to inspect the ICA region in its natural and dynamic states. Being a noncontact technique, the risk of corneal infection or abrasion is minimal for the patients and hence is suitable for pre- and postoperative ocular imaging and even for cases with prior ocular injuries, in contrast with other imaging techniques like confocal microscopy or UBM. The advantages of the proposed prototype are summarized in Table 3.

A direct view of the ICA region is not possible because it is obstructed by the sclera overlap. Therefore, viewing the TM structures from the opposite angle is the best method to observe them. The resulting images obtained from the ICA region of the porcine sample (ex vivo) and NZW rabbit (in vivo) using the proposed optical imaging prototype are shown in Figures 6a and b, respectively. In contrast with the heavily pigmented porcine eye, the NZW rabbits have a genetic deviation known as albinism. The high-resolution images obtained using this prototype can be attributed to the Bessel beam's ability to reconstruct through scattering media. This unique characteristic of the Bessel beam helps in obtaining a high-contrast image of the TM network, and helps in minimizing shadowing and scattering artifacts.[24,38] The collagen

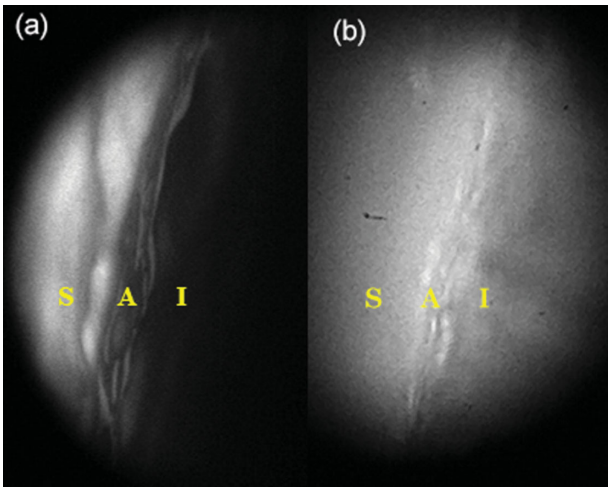

Figure 6. (a) Two-dimensional images of porcine ICA region (ex vivo) and (b) NZW rabbit ICA region (in vivo) recorded using the proposed Bessel LSFM imaging system. A, ICA; I, iris; S, sclera. The network arrangement of the TM can be seen in both the images.

fiber network of the TM can be clearly seen in the obtained images. The dimensional features match well with previous histologic measurements reported in the literature.[39–41] The imaging contrast in Figure 6b is lower compared with the image in Figure 6a owing to motion artifacts, and shorter exposure times used to decrease the motion artifacts.

Corneal Imaging

A long working distance objective at the distal end is highly desirable and often necessary for ocular imaging, to avoid epithelial injury and to minimize patient discomfort. Because the working distance of an objective decreases as its magnification and NA increases, it can be understood that the working distance of an objective is limited by the need for a high NA and, hence, a high resolving power. The lateral resolution of the optical setup for corneal imaging is given by the conventional wide field microscopy diffraction limit. Although the same objective lens was used, the lateral resolution is slightly different compared with the optical setup used for ICA imaging owing to the change in excitation wavelength. Although a higher magnification offers better lateral resolution, it comes at the expense of the working distance and the region of interest. This is because the FOV of the proposed configuration is limited by the inverse ratio of the objective magnification and the field number of the scan lens.[42] The maximum FOV achievable with the 20× objective lens in this prototype is approximately 1.3 mm.

The noncontact and upright positioning of the sample as well as near infrared illumination, enable viewing the cornea in its dynamic and natural states. The proposed prototype does not require any complicated sample preparation or coupling medium. These eliminate the risk of exposing the patient to the infections and corneal abrasion associated with contact procedures. In contrast with confocal microscopy and UBM, this procedure is thus would be applicable to patients with ocular injuries, as well as for pre- and postoperative eyes. As in the case of OCTs, the area of the sulcus is not visible owing to the inability of the infrared light to penetrate the posterior layer of the iris, and the ciliary body cannot be imaged owing to absorption of the infrared light through the sclera. The proposed optical setup combines the high spatial resolution of confocal microscopy with the noncontact feature of the OCTs. Furthermore, the proposed setup is easily portable and nonbulky, and is compatible with any workstation that is equipped with the interfacing software. Both single frame acquisition and kinetic series recording are available depending on the users' preference. However, because the proposed system uses a lower wavelength for illumination compared with other imaging modalities like OCT, it has a lower penetration depth owing to the higher scattering from ocular tissues. It should also be noted that high illumination powers are undesirable in the proposed system owing to the lower absorption by water in ocular media at this wavelength, which results in decreased retinal protection.[43] The lower illumination power constraints the imaging speed of the system. Nonetheless, because the proposed system makes use of a high-speed and high-sensitivity CMOS camera, this factor is not much of a concern. Moreover, the use of shorter wavelength results in a higher lateral resolution based on conventional wide field microscopy diffraction limit, given by $\lambda_{ex}/(2NA_{det})$.

Under the proposed scheme, using a scan speed of 50 μm/s, it takes approximately 15 s to cover the entire corneal thickness of the porcine eye, whereas it takes approximately 6 s to cover the entire thickness of rabbit cornea. It is estimated to take approximately 7 s to scan the entire thickness of the human cornea, because the average thickness of human cornea is approximately 500 μm.[44] Figure 7 shows the images of the porcine and rabbit corneas captured across the entire thickness. The excitation intensity was always kept lower than the maximum permissible exposure limit advocated by the International Commission on Non-Ionizing Radiation Protection and the American National Standards Institute.[45,46] Subsequent confocal microscope images on the rabbit cornea also show that no damage were induced due to the laser excitation. The corneal images acquired from porcine eyes (ex vivo) and NZW rabbit (in vivo) using the developed system are presented in Figure 7.

Motion artefact was one of the challenges faced during the in vivo imaging of the rabbit cornea. Even though the measurements were conducted when the rabbit was under general anesthesia, the motion caused by its breathing between image acquisitions resulted in significant motion artefacts. This factor, however, was not a concern with ex vivo porcine eyes. These motion artefacts can be reduced further through fixation targets and averaging techniques, along with postprocessing edits. We would like to note here that, owing to the slow scanning speed of the system, it may not be feasible to image the entire cornea during in vivo measurements using this technique. We rather envision this system to complement standard ophthalmic techniques, such as AS-OCT, with high-resolution images of specific regions of interest.

The acquired corneal images show the cellular structures of the cornea. In this epi-illumination configu-

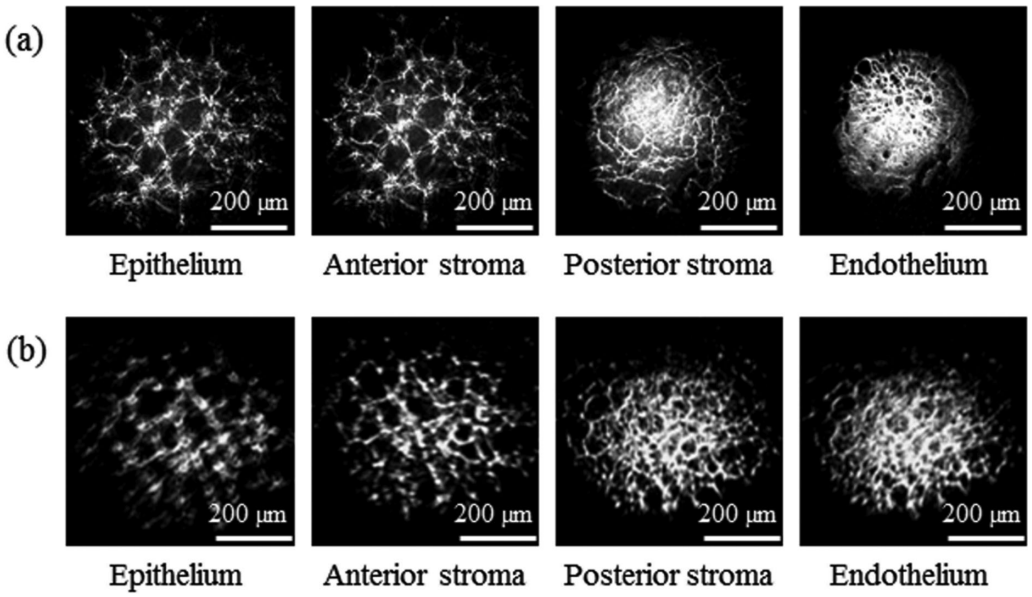

Figure 7. Unprocessed digital images of the (a) porcine (ex vivo) and (b) NZW rabbit (in vivo) corneas captured across the entire thickness. The individual layers' images are overlapped with the out-of-focus images in these frames.

Table 4. Comparison of Different Ophthalmologic Imaging Techniques

Imaging Technique	Noncontact Imaging	High Resolution (<5 µm)	Imaging Cornea	Imaging TM	Measurement Principle
AS-OCT	Yes	Yes	Yes	Limited	Interferometry
LSCM	No	Yes	Yes	No	Confocal microscopy
Multiphoton	Yes	Yes	Yes	Yes	Multiphoton fluorescence
UBM	No	No	Yes	No	Ultrasound imaging
Gonioscopy	No	No	Yes	Limited	Microscopy
Reported Prototype	Yes	Yes	Yes	Yes	Light sheet fluorescence

ration, the amount of optical backscatter depends on the changes in refractive indices between the different layers within the cornea. Greater changes in the refractive index results in a higher reflectance that in turn leads to a larger contrast difference. The 3D profile of the entire cornea can be reconstructed from the depth measurements. However, further system modification and postacquisition image processing are necessary because of the proposed system's inability to eliminate out-of-focus blurs caused by light emanating from regions below and above the focal plane. This explains why the images seem to be obscured at the endothelium layer. Another limitation of the proposed system is that the two-dimensional topography is unable to capture the entire cornea in a single acquisition. The average corneal diameter of a healthy adult is approximately 11.7 mm.[47] With a FOV of approximately 1.3 mm, it takes about nine individual acquisitions to scan across the diameter of the cornea. A comparison of the developed prototype's capabilities with some of the standard ophthalmologic imaging devices is presented in Table 4.

Conclusion

A noninvasive and noncontact ocular imaging system for the sequential imaging of the cornea and ICA has been demonstrated based on a Gaussian beam epi-illumination configuration, and a Bessel beam plane illumination configuration, respectively. The acquired images can be saved into a computer database, which will allow clinicians to engage in continuous evaluation of the disease progression and response to the treatment over time. Preliminary studies on animal models show promising results.

The proposed corneal imaging prototype has cellular-level imaging resolution, and it would be useful to incorporate analytical tools for pachymetry and keratometry readings in the next prototype.

The transcorneal ICA imaging configuration using the Bessel beam virtual light sheet can surpass the trade-off between length and thickness of a conventional Gaussian light sheet and thus results in better axial resolution with improved signal-to-noise ratio. Although various configurations of light sheet microscopy have been widely used in developmental biology,[48–50] we are the first to report the application of LSFM in the field of ophthalmology.[26] The spatial resolution of the proposed system is adequate enough to image the TM structures and thus can provide objective information about the AOS. The use of high-speed, high photon efficiency scientific complementary metal-oxide semiconductor camera allows subcellular spatial resolution both ex vivo and in vivo. Nonetheless, it must be noted that live fluorescence imaging is usually limited to two-dimensional images over limited time intervals. This incomplete representation of biological samples can be misleading to clinicians and vision researchers for an objective evaluation of glaucoma. By sweeping the Bessel beam in x-direction to project a light sheet at each z-plane, a 3D volumetric stack can be created.[51] The sample under study should be kept stationary throughout this 3D data acquisition, which will help in minimizing motion artifacts. Such motion artefacts will be lesser in human eye imaging compared with animals under anesthesia. Another limitation in the TM imaging scheme is that the deeper structures of the AOS, such as the Schlemm's canal, are not resolved owing to the low penetration depth of the illumination wavelength. Combining OCT or other imaging modalities to the proposed scheme could be a future solution in this regard.

The proposed corneal imaging scheme is able to resolve individual cellular structures of the cornea. This scheme potentially enables the identification and characterization of infectious agents during an inflammatory response or cellular-level responses to pathologic processes, even in cases of abnormalities or corneal opacities. Clinicians and vision researchers can therefore classify the disease states without the need to mechanically remove samples from the cornea. This allows the objective evaluation of subsequent treatment response, and also contributes to the cost effectiveness.

More translational and clinical investigations are necessary to determine the effectiveness of the proposed method in a clinical setting to complement existing imaging modalities. Comparative studies with other established methodologies can improve the effectiveness of subsequent treatments and decrease morbidity. Being a simple, noncontact and high-resolution method, the proposed methodology is envisaged to be a useful tool for clinicians for the diagnosis and management of corneal diseases and glaucoma by complimenting existing tools such as AS-OCT with zoomed in views of the areas of interest.

Acknowledgments

The authors acknowledge financial support received through A*STAR-MIG project (BMRC1619077002), NMRC Transition Award (NMRC/TA/0040/2015), and A*STAR-SERC grant (1121480003) for pursuing part of the contents presented in this article, and the research manpower and facilities provided through COLE-EDB funding at COLE, NTU. The authors thank Nyein Chan Lwin from SERI for assistance with in vivo measurements. The authors hold a Singapore patent (WO/2016/137396) and a US patent (20180078129) on the design aspect and imaging methodology of the probe scheme described in this manuscript. S.V.K. contributed to this work when he was a research staff at the School of Mechanical and Aerospace Engineering, Nanyang Technological University. This research is also supported by the Singapore Ministry of Health's National Medical Research Council under its NMRC Centre Grant (CG-Imaging) Programme (NMRC/CG/C010A/2017/PreClinical).

Disclosure: **X.J.J. Hong**, None; **C.S. Suchand Sandeep**, None; **V.K. Shinoj**, None; **T. Aung**, None; **V.A. Barathi**, None; **M. Baskaran**, None; **V.M. Murukeshan**, None

References

1. Oliver JE, Hattenhauer MG, Herman D, et al. Blindness and glaucoma: a comparison of patients progressing to blindness from glaucoma with patients maintaining vision. *Am J Ophthalmol*. 2002;133:764–772.
2. V K S, Hong XJ, V M M, M B, Tin A. Progress in anterior chamber angle imaging for glaucoma risk prediction – A review on clinical equipment, practice and research. *Med Eng Phys*. 2016;38:1383–1391.
3. Huang D, Swanson EA, Lin CP, et al. Optical coherence tomography. *Science*. 1991;254:1178–1181.
4. Leung CK, Li H, Weinreb RN, et al. Anterior chamber angle measurement with anterior segment optical coherence tomography: a comparison between slit lamp OCT and Visante OCT. *Invest Ophthalmol Vis Sci*. 2008;49:3469–3474.

5. Ang M, Baskaran M, Werkmeister RM, et al. Anterior segment optical coherence tomography. *Prog Retin Eye Res*. 2018;66:132–156.
6. Yasuno Y, Yamanari M, Kawana K, et al. Visibility of trabecular meshwork by standard and polarization-sensitive optical coherence tomography. *J Biomed Opt*. 2010;15:061705.
7. Xin C, Johnstone M, Wang N, Wang RK. OCT study of mechanical properties associated with trabecular meshwork and collector channel motion in human eyes. *PLoS One*. 2016;11:e0162048.
8. Dada T, Mohan S, Sihota R, Gupta R, Gupta V, Pandey RM. Comparison of ultrasound biomicroscopic parameters after laser iridotomy in eyes with primary angle closure and primary angle closure glaucoma. *Eye (Lond)*. 2007;21:956–961.
9. Perinchery SM, Shinde A, Fu CY, et al. High resolution iridocorneal angle imaging system by axicon lens assisted gonioscopy. *Sci Rep*. 2016;6:30844.
10. Resnikoff S, Pascolini D, Etya'ale D, et al. Global data on visual impairment in the year 2002. *Bull World Health Org*. 2004;82:844–851.
11. Whitcher JP, Srinivasan M, Upadhyay MP. Corneal blindness: a global perspective. *Bull World Health Org*. 2001;79:214–221.
12. Patel DV, McGhee CN. In vivo laser scanning confocal microscopy confirms that the human corneal sub-basal nerve plexus is a highly dynamic structure. *Invest Ophthalmol Vis Sci*. 2008;49:3409–3412.
13. Ishikawa H, Inazumi K, Liebmann J, Ritch R. Inadvertent corneal indentation can cause artifactitious widening of the iridocorneal angle on ultrasound biomicroscopy. *OSLI Retina*. 2000;31:342–345.
14. Teng SW, Tan HY, Peng JL, et al. Multiphoton autofluorescence and second-harmonic generation imaging of the ex vivo porcine eye. *Invest Ophthalmol Vis Sci*. 2006;47:1216–1224.
15. Avila FJ, Gambin A, Artal P, Bueno JM. In vivo two-photon microscopy of the human eye. *Sci Rep*. 2019;9:10121.
16. Izatt JA, Hee MR, Swanson EA, et al. Micrometer-scale resolution imaging of the anterior eye in vivo with optical coherence tomography. *Arch Ophthalmol*. 1994;112:1584–1589.
17. Tan B, Hosseinaee Z, Han L, Kralj O, Sorbara L, Bizheva K. 250 kHz, 1.5 micron resolution SD-OCT for in-vivo cellular imaging of the human cornea. *Biomed Opt Express*. 2018;9:6569–6583.
18. Chen S, Liu X, Wang N, et al. Visualizing micro-anatomical structures of the posterior cornea with micro-optical coherence tomography. *Sci Rep*. 2017;7:10752.
19. Thouvenin O, Grieve K, Xiao P, Apelian C, Boccara AC. En face coherence microscopy [Invited]. *Biomed Opt Express*. 2017;8:622–639.
20. James J, Murukeshan VM, Woh LS. Integrated photoacoustic, ultrasound and fluorescence platform for diagnostic medical imaging-proof of concept study with a tissue mimicking phantom. *Biomed Opt Express*. 2014;5:2135–2144.
21. Xia Y, Matham MV, Su H, Padmanabhan P, Gulyas B. Nanoparticulate contrast agents for multimodality molecular imaging. *J Biomed Nanotechnol*. 2016;12:1553–1584.
22. Durnin J. Exact solutions for nondiffracting beams. I. The scalar theory. *JOSA A*. 1987;4:651–654.
23. Durnin J, Miceli J, Jr., Eberly JH. Diffraction-free beams. *Phys Rev Lett*. 1987;58:1499–1501.
24. Fahrbach FO, Simon P, Rohrbach A. Microscopy with self-reconstructing beams. *Nat Photonics*. 2010;4:780–785.
25. Hong XJ, Shinoj VK, Murukeshan VM, Baskaran M, Aung T. A simple and non-contact optical imaging probe for evaluation of corneal diseases. *Rev Sci Instrum*. 2015;86:093702.
26. Hong X, Shinoj V, Murukeshan V, Baskaran M, Aung T. Imaging of trabecular meshwork using Bessel–Gauss light sheet with fluorescence. *Laser Phys Lett*. 2017;14:035602.
27. Gray JR, Mosier MA, Ishimoto BM. Optimized protocol for Fluorotron Master. *Graefes Arch Clin Exp Ophthalmol*. 1985;222:225–229.
28. Arimoto R, Saloma C, Tanaka T, Kawata S. Imaging properties of axicon in a scanning optical system. *Appl Opt*. 1992;31:6653–6657.
29. Born M, Wolf E. *Principles of Optics*, 7th (expanded) ed. Cambridge: Cambridge University Press; 1999;517ˆ#x2013;547.
30. Kumar M, Kozorovitskiy Y. Tilt-invariant scanned oblique plane illumination microscopy for large-scale volumetric imaging. *Opt Lett*. 2019;44:1706–1709.
31. Calkins L. The aqueous filtration angle: a phylogenetic and ontogenetic comparative histo-anatomic study of mammalian eyes. *Trans Am Ophthalmol Soc*. 1960;58:364–391.
32. Ruiz-Ederra J, Garcia M, Hernandez M, et al. The pig eye as a novel model of glaucoma. *Exp Eye Res*. 2005;81:561–569.
33. Faber C, Wang M, Scherfig E, et al. Orthotopic porcine corneal xenotransplantation using a human graft. *Acta Ophthalmol*. 2009;87:917–919.

34. Jay L, Brocas A, Singh K, Kieffer JC, Brunette I, Ozaki T. Determination of porcine corneal layers with high spatial resolution by simultaneous second and third harmonic generation microscopy. *Opt Express*. 2008;16:16284–16293.
35. Kolker AE, Moses RA, Constant MA, Becker B. The development of glaucoma in rabbits. *Invest Ophthalmol*. 1963;2:316–321.
36. Bozkir G, Bozkir M, Dogan H, Aycan K, Guler B. Measurements of axial length and radius of corneal curvature in the rabbit eye. *Acta Med Okayama*. 1997;51:9–11.
37. Hayashi S, Osawa T, Tohyama K. Comparative observations on corneas, with special reference to Bowman's layer and Descemet's membrane in mammals and amphibians. *J Morphol*. 2002;254:247–258.
38. Fahrbach FO, Rohrbach A. Propagation stability of self-reconstructing Bessel beams enables contrast-enhanced imaging in thick media. *Nat Commun*. 2012;3:632.
39. Latina MA, Park C. Selective targeting of trabecular meshwork cells: in vitro studies of pulsed and CW laser interactions. *Exp Eye Res*. 1995;60:359–371.
40. Masihzadeh O, Ammar DA, Kahook MY, Gibson EA, Lei TC. Direct trabecular meshwork imaging in porcine eyes through multiphoton gonioscopy. *J Biomed Opt*. 2013;18:036009.
41. Gibson EA, Masihzadeh O, Lei TC, Ammar DA, Kahook MY. Multiphoton microscopy for ophthalmic imaging. *J Ophthalmol*. 2011;2011:870879.
42. Krzic U, Gunther S, Saunders TE, Streichan SJ, Hufnagel L. Multiview light-sheet microscope for rapid in toto imaging. *Nat Methods*. 2012;9:730–733.
43. van den Berg TJ, Spekreijse H. Near infrared light absorption in the human eye media. *Vision Res*. 1997;37:249–253.
44. Doughty MJ, Zaman ML. Human corneal thickness and its impact on intraocular pressure measures: a review and meta-analysis approach. *Surv Ophthalmol*. 2000;44:367–408.
45. Sliney D, Aron-Rosa D, DeLori F, et al. Adjustment of guidelines for exposure of the eye to optical radiation from ocular instruments: statement from a task group of the International Commission on Non-Ionizing Radiation Protection (ICNIRP). *Appl Opt*. 2005;44:2162–2176.
46. Delori FC, Webb RH, Sliney DH. Maximum permissible exposures for ocular safety (ANSI 2000), with emphasis on ophthalmic devices. *J Opt Soc Am A Opt Image Sci Vis*. 2007;24:1250–1265.
47. Rufer F, Schroder A, Erb C. White-to-white corneal diameter: normal values in healthy humans obtained with the Orbscan II topography system. *Cornea*. 2005;24:259–261.
48. Verveer PJ, Swoger J, Pampaloni F, Greger K, Marcello M, Stelzer EH. High-resolution three-dimensional imaging of large specimens with light sheet-based microscopy. *Nat Methods*. 2007;4:311–313.
49. Planchon TA, Gao L, Milkie DE, et al. Rapid three-dimensional isotropic imaging of living cells using Bessel beam plane illumination. *Nat Methods*. 2011;8:417–423.
50. Ahrens MB, Orger MB, Robson DN, Li JM, Keller PJ. Whole-brain functional imaging at cellular resolution using light-sheet microscopy. *Nat Methods*. 2013;10:413–420.
51. Suchand Sandeep CS, Sarangapani S, Hong XJJ, Aung T, Baskaran M, Murukeshan VM. Optical sectioning and high resolution visualization of trabecular meshwork using Bessel beam assisted light sheet fluorescence microscopy. *J Biophotonics*. 2019;12:e201900048.